Journal of Power Sources 195 (2010) 4997–5004

Contents lists available at ScienceDirect

Journal of Power Sources

journal homepage: www.elsevier.com/locate/jpowsour

Synthesis of pristine and carbon-coated $Li_4Ti_5O_{12}$ and their low-temperature electrochemical performance

Tao Yuan, Xing Yu, Rui Cai, Yingke Zhou, Zongping Shao*

State Key Laboratory of Materials-Oriented Chemical Engineering, College of Chemistry & Chemical Engineering, Nanjing University of Technology, No. 5 Xin Mofan Road, Nanjing, 210009, PR China

ARTICLE INFO

Article history:
Received 19 December 2009
Received in revised form 7 February 2010
Accepted 8 February 2010
Available online 17 February 2010

Keywords:
Lithium titanate
Combustion synthesis
Anode
Low temperature
Carbon-coated

ABSTRACT

Pristine and carbon-coated $Li_4Ti_5O_{12}$ oxide electrodes are synthesized by a cellulose-assisted combustion technique with sucrose as organic carbon source and their low-temperature electrochemical performance as anodes for lithium-ion batteries are investigated. X-ray diffraction (XRD), infrared spectroscopy (IR), Raman spectroscopy, thermogravimetric analysis (TGA) and scanning electron microscopy (SEM) are applied to characterize the phase structure, composition, and morphology of the composites. It is found that the sequence of sucrose addition has significant effect on the phase formation of $Li_4Ti_5O_{12}$. Carbon-coated $Li_4Ti_5O_{12}$ is successfully prepared by coating the pre-crystallized $Li_4Ti_5O_{12}$ phase with sucrose followed by thermal treatment. Electrochemical lithium insertion/extraction performance is evaluated by the galvanostatic charge/discharge tests, electrochemical impedance spectroscopy (EIS), and cyclic voltammetry (CV), from room temperature (25 °C) to −20 °C. The carbon-coated composite anode materials show improved lithium insertion/extraction capacity and electrode kinetics, especially at high rates and low temperature. Both of the two samples show fairly stable cycling performance at various temperatures, which is highly promising for practical applications in power sources of electric or electric-hybrid vehicles.

1. Introduction

$Li_4Ti_5O_{12}$ belongs to the family of Li–Ti–O solid solutions with a spinel-type phase structure [1,2], which has received considerable attention recently as a potential anode material of rechargeable lithium-ion battery because of its several outstanding features. $Li_4Ti_5O_{12}$ shows a favorable theoretical capacity of around 175 mAh g^{-1} [3,4]. It has near zero volume change during the charge/discharge processes which ensures a long cycling life [5]. The lithium insertion into and extraction from $Li_4Ti_5O_{12}$ follows a two-phase mechanism, which gives an ultra-flat operating voltage of around 1.5 V versus Li/Li^+ [6,7], above the reduction potential of common electrolyte solvents thus, solid electrolyte interface based on solvent reduction is unlikely to occur, furthermore, the voltage is sufficiently high to remove the possibility for lithium plating.

For security and cycling stability concerns, $Li_4Ti_5O_{12}$ is highly promising for high rate and low-temperature operation. The electrode processes involve the lithium-ion and electron diffusion within the electrode interior and the surface charge transfers. However, $Li_4Ti_5O_{12}$ has poor electronic and lithium ionic conductivity (σ_e and σ_{Li^+}), the reported σ_e and σ_{Li^+} values of $Li_4Ti_5O_{12}$ at room temperature are 10^{-13} S cm^{-1} and 10^{-12} cm^2 s^{-1}, respectively [2,8]. The low electrical conductivity results in a sluggish electrode kinetic, as a result, coarse $Li_4Ti_5O_{12}$ typically shows large electrode polarization resistance at high charge/discharge rate so poor rate performance.

Nowadays, people are trying to increase the rate performance of $Li_4Ti_5O_{12}$ anode by various strategies [9–19]. Reducing the particles size by advanced synthesis and surface coating of the electrode with porous carbons are the two most frequently adopted ways. The reduction in particle size can not only increase the active sites for surface reactions, but also reduces the distance for lithium and electron diffusion within the electrode bulk. As a result a substantial increase in rate performance was frequently observed [13–19]. Surface coating of the electrode material with a porous carbon layer or other conducting oxide/metal was also investigated [20–25]. Obvious improvement in electrical conductivity was observed, sometimes an increment in apparent electrical conductivity by several orders of magnitude was achieved [20,21]. Through the formation of $Li_4Ti_5O_{12}$/C composite, a significant improvement in rate performance was reported [24,25].

For practical application, the lithium-ion batteries may often be used in low-temperature environment, especially as power sources of electric or electric-hybrid vehicles. With the drop of operation

* Corresponding author. Tel.: +86 25 83172256; fax: +86 25 83172256.
E-mail address: shaozp@njut.edu.cn (Z. Shao).

0378-7753/$ – see front matter © 2010 Elsevier B.V. All rights reserved.
doi:10.1016/j.jpowsour.2010.02.020

temperature, both the surface reaction kinetics and the rate of charge (lithium-ion and electron) diffusion inside the electrode bulk are slowed down. Thereby, a bigger challenge for the electrode is expected. Up to now, however, there are rare reports about the low-temperature performance of $Li_4Ti_5O_{12}$. The only available related research work in the literature was reported by Allen et al. [26]. They investigated the effect of particle size on the performance of $Li_4Ti_5O_{12}$ at room and reduced temperatures. From a general sense, a better performance should be expected for the electrode with smaller size. Indeed it was observed at high rate and room temperature or at low temperature and low rate, and $Li_4Ti_5O_{12}$ with a particle size of 350 nm has higher capacity than the 700 nm $Li_4Ti_5O_{12}$, however, at low temperature and high rate, the 700 nm sample showed higher capacity. They proposed that the inter-particle contact resistance becomes the rate limiting issue at low temperature and high rate. It was well known that the wiring of particles becomes more difficult with the decrease of particle size. The surface coating with carbon increases the apparent electrical conductivity greatly, which may improve the current collecting efficiency obviously. So an improvement in electrode performance is expected.

Previously we developed a cellulose-assisted combustion technique for the synthesis of fine $Li_4Ti_5O_{12}$ which showed exciting high rate performance at room temperature [19]. In this study, carbon-coated $Li_4Ti_5O_{12}$ ($Li_4Ti_5O_{12}$/C) was further synthesized by the modified technique using sucrose as an organic carbon source, and its low-temperature electrochemical performance was comparatively studied with the pristine $Li_4Ti_5O_{12}$. The improved electrode performance from the carbon coating was observed and the effects of carbon were discussed and explained.

2. Experimental

2.1. Materials synthesis

$Li_4Ti_5O_{12}$ oxide was prepared by a cellulose-assisted combustion process with titanium (IV) butoxide [$Ti(C_4H_9O)_4$] as the titanium source, the detailed preparation procedure can refer to our previous publication [19]. For the preparation of carbon-coated $Li_4Ti_5O_{12}$ ($Li_4Ti_5O_{12}$/C), sucrose was selected as the carbon source. The raw materials were weighed in stoichiometric amounts according to the nominal $Li_4Ti_5O_{12}$ to C weight ratio 95 to 5, assuming the sucrose following the thermal pyrolysis reaction $C_{12}H_{22}O_{11} \rightarrow 12C + 11H_2O$.

2.2. Electrode fabrication

The electrochemical performance of the as-synthesized $Li_4Ti_5O_{12}$ or $Li_4Ti_5O_{12}$/C composite was carried out with coin-shape cells using metallic lithium film as the counter and reference electrode. The cells are based on the configuration of Li metal (−) |electrolyte| $Li_4Ti_5O_{12}$ (+) with a liquid electrolyte (1 M solution of $LiPF_6$ in ethylene carbonate (EC)-dimethyl carbonate (DMC) (1:1, v/v)). Microporous polypropylene film (Celgard 2400) was used as the separator. 85 wt.% $Li_4Ti_5O_{12}$ with 8 wt.% conductive carbon Super P (NCM HERSBIT Chemical Co., Ltd., China) and 7 wt.% polyvinylidene fluoride (PVDF) binder homogeneously mixed in N-methyl pyrrolidinone (NMP) were prepared into viscous slurries for efficient deposition. The slurries were deposited on current collectors of copper foil (10 μm) by blade, which was pretreated by etching with 1 M nitric acid solutions followed by rinsing with water and then acetone. The electrode was then dried under vacuum at 100 °C for 12 h before electrochemical evaluation. Cell assembly was conducted in a glove box filled with pure argon.

2.3. Basic analysis

The crystal structures of the synthesized powders were examined by X-ray diffraction (XRD) using a Bruker D8 advance diffractometer with filtered Cu Kα radiation. The experimental diffraction patterns were collected at room temperature by step scanning in the range of $10^\circ \leq 2\theta \leq 80^\circ$. The particle morphology was examined by Environmental Scanning Electronic Microscope (ESEM, QUANTA-2000). The specific surface area of the samples was characterized by N_2 adsorption at the temperature of liquid nitrogen using a BELSORP II instrument. Prior to analysis, the samples were treated at 100 °C for 3–5 h in vacuum to remove the surface adsorbed species. Fourier transform infrared spectroscopy (FT-IR, AVATAR-360) of the solid precursors or the calcinated samples was recorded from 4000 to 400 cm^{-1} by the KBr pellet method. Thermogravimetry-differential scanning calorimetric analysis (TG-DSC) was performed using a NETZSCH STA 409 PC in the range of 25–800 °C at a heating rate of 10 °C min^{-1} under flowing air atmosphere. The Raman spectroscopy of the $Li_4Ti_5O_{12}$/C was obtained in an HR800 UV Raman micro-spectrometer (JOBIN YVON, France) using the green line of an argon laser (λ = 514.53 nm) as excitation source.

2.4. Electrochemical characterization

The charge–discharge characteristics of the cells were recorded over the potential range between 1.0 and 3.0 V using a NEWARE BTS-5V50 mA computer-controlled battery test station at different rates of 1–40 C. Cyclic voltammetry tests were performed over the potential range of 1.0–3 V using a Princeton Applied Research PARSTAT 2273 advanced electrochemical system. Complex impedance measurements were also carried out using Princeton 2273 electrochemical system over the single cell at the state of discharging (1.6 V). A perturbation of 10 mV was applied and data collected under PC control and the frequency range applied is from 1 MHz to 100 mHz. A digital low-temperature biochemical incubator was used to provide constant temperature at 25, 0, −10, and −20 °C.

3. Results and discussion

3.1. Synthesis

By applying the cellulose-assisted combustion technique with titanium (IV) butoxide [$Ti(C_4H_9O)_4$] as the raw material, a phase-pure spinel-type $Li_4Ti_5O_{12}$ was successfully obtained by firing the primary powder from auto-combustion at 700 °C for 5 h in air [19]. In this study, the same technique was also applied for the synthesis of the pristine $Li_4Ti_5O_{12}$. For the synthesis of 5.00 g $Li_4Ti_5O_{12}$, 3.01 g $LiNO_3$ and 18.53 g $Ti(C_4H_9O)_4$ were impregnated into ∼8 g nitric acid-activated cotton, after drying the solid precursor was auto-combusted by heating at 250 °C, the primary powder obtained from the auto-combustion was further fired at 700 °C for 5 h. As shown in Fig. 1a, all the diffraction peaks of the as-synthesized powder can be well indexed based on a spinel-type lattice structure with cubic symmetry, no other diffraction peak assignable to impurity phase was observed, it suggests the successful formation of a phase-pure $Li_4Ti_5O_{12}$, in good agreement with our previous report [19]. For a solid-state reaction, a calcination at 850 °C for a prolonged period of 17 h, or a calcination at 950 °C for 5 h is needed to obtain a phase-pure $Li_4Ti_5O_{12}$ [27,28]. The reduced synthesis temperature via the cellulose-assisted combustion technique was attributed to the homogeneous mixing of the raw materials in the precursor and the promoting effect of cellulose on the combustion.

Sucrose was applied for the formation of $Li_4Ti_5O_{12}$/C composite, since it has been often adopted as an organic carbon source for

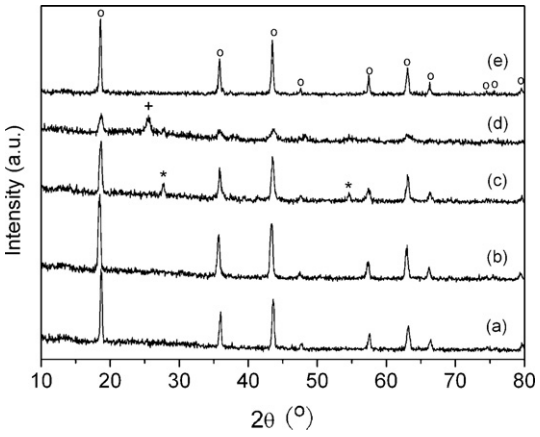

Fig. 1. X-ray diffraction patterns of the (a) $Li_4Ti_5O_{12}$ prepared by cellulose-assisted combustion process calcined at 700 °C for 5 h in air; (b) $Li_4Ti_5O_{12}$/C from way-1; (c) $Li_4Ti_5O_{12}$/C from way-2; (d) sample from cellulose-assisted combustion process calcined at 400 °C for 5 h in air; (e) further calcination of the 400 °C calcined sample at 700 °C for 5 h in air. (o): spinel $Li_4Ti_5O_{12}$, (+): anatase TiO_2 and (*): rutile TiO_2.

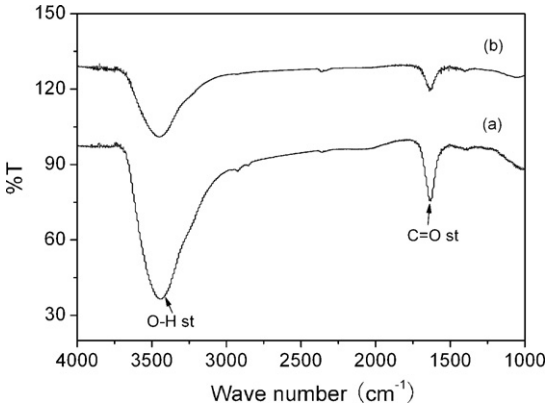

Fig. 2. FT-IR spectra of (a) $Li_4Ti_5O_{12}$ and (b) $Li_4Ti_5O_{12}$/C sample.

the in situ creation of carbon coating because of its low pyrolysis temperature [29]. Two ways were investigated. One way is to mix sucrose with phase-pure $Li_4Ti_5O_{12}$, prepared from the cellulose-assisted combustion synthesis after the calcination at 700 °C for 5 h, by ball milling, and then the mixture was fired at 700 °C in an inert atmosphere to allow the thermal decomposition of sucrose to solid carbon (way-1). For the other way (way-2), the primary powder from the cellulose-assisted combustion synthesis was pre-fired at 400 °C instead of 700 °C, the powder was then mixed with sucrose through ball milling in acetone liquid medium for 1 h, and then the mixture was fired at 700 °C in nitrogen for 5 h for the decomposition of sucrose to solid carbon. The pre-firing at 400 °C is on the purpose to suppress the grain growth of the product. Fig. 1b and c shows the X-ray diffraction patterns of the $Li_4Ti_5O_{12}$/C synthesized from way-1 and way-2, respectively. For the powder from way-1, all the diffraction peaks can be indexed well based on a spinel-type lattice structure with no any peak assignable to crystallized carbon. It suggests that the $Li_4Ti_5O_{12}$ phase was survived and the formed carbon was likely in amorphous structure. As to the powder from way-2, besides the main spinel-type phase, some diffraction peaks assignable to the TiO_2 rutile phase were also observed. To demonstrate the cause for the formation of TiO_2 rutile phase via way-2, the phase structure of the powder from calcination at 400 °C was also examined with the result shown in Fig. 1d. TiO_2 anatase phase was formed alongside with the spinel-type phase. It suggests that the titanium alkoxide was first transformed into TiO_2 anatase phase before the formation of the $Li_4Ti_5O_{12}$ phase. Previously we have demonstrated that the competitive reactions of phase transition of TiO_2 from anatase to rutile and the phase reaction of TiO_2 with lithium for the formation of $Li_4Ti_5O_{12}$ happened during the high-temperature calcination for the synthesis of $Li_4Ti_5O_{12}$ from TiO_2 anatase [30]. Since the phase transition of TiO_2 from anatase to rutile did not involve long distance cation diffusion, it is more easily to occur as compared to the reaction between TiO_2 and Li with the formation of $Li_4Ti_5O_{12}$. Once TiO_2 rutile was formed, the formation of $Li_4Ti_5O_{12}$ was suppressed since its much worse reactivity than TiO_2 anatase. When no sucrose was introduced during the synthesis, phase-pure $Li_4Ti_5O_{12}$ was still obtained by further calcination of the 400 °C calcined sample at 700 °C for 5 h, as shown in Fig. 1e. It suggests that the homogeneous mixing and the fine size of lithium and TiO_2 from the cellulose-assisted combustion synthesis, which effectively reduced the diffusion distance for the formation of $Li_4Ti_5O_{12}$.

The formation of TiO_2 rutile by introducing sucrose during the synthesis could then be explained as follows. After the calcination at 400 °C, the titanium alkoxide was transformed to TiO_2 anatase solid, the introduction of sucrose as the organic carbon source through high energy ball milling made the sucrose cover the TiO_2 and lithium surfaces and act as a diffusion block for the cations, as a result, the reaction of lithium with TiO_2 towards the formation of $Li_4Ti_5O_{12}$ was suppressed. As to the phase transformation of TiO_2 from anatase to rutile, since it did not involve the cation diffusion, the carbon coating should have no impact on the reaction rate. It suggests the TiO_2 preferred to transform to TiO_2 rutile instead of reacting with lithium towards the formation of $Li_4Ti_5O_{12}$ when sucrose was adopted during the synthesis. Once rutile TiO_2 was formed, the formation of $Li_4Ti_5O_{12}$ was further suppressed since its much worse reactivity than TiO_2 anatase. As a result, it was failed to obtain a phase-pure $Li_4Ti_5O_{12}$ by way-2. In the following studies, way-1 was applied for the synthesis of carbon-coated $Li_4Ti_5O_{12}$.

To demonstrate whether a calcination time of 2 h at 700 °C is sufficient for the full decomposition of sucrose into solid carbon, the pristine $Li_4Ti_5O_{12}$ and the $Li_4Ti_5O_{12}$/C prepared from way-1 were subjected for FT-IR analysis. As shown in Fig. 2, similar to the pristine TiO_2, there were only two absorption bands appeared between 1000 and 4000 cm^{-1}, one at around 1700 cm^{-1} and the other broad band at 3450 cm^{-1}, which are assigned to the stretch vibration of C=O band, and the stretch vibration of O–H originated probably from the humidity effect of KBr medium [31], respectively. There were no absorption bands assignable to the C–O and C–H vibration bands were detected, which is a strong sign of the total decomposition of sucrose.

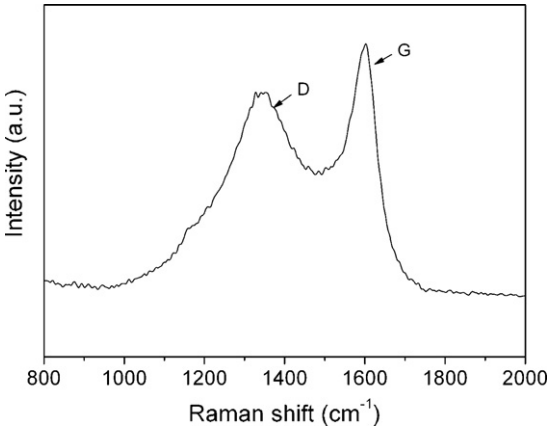

Fig. 3. Raman spectra of $Li_4Ti_5O_{12}$/C powder.

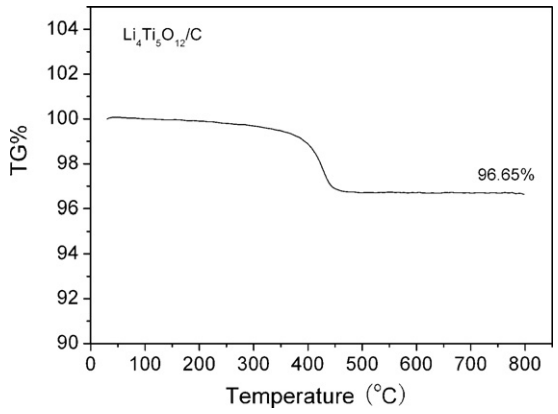

Fig. 4. TGA curve of $Li_4Ti_5O_{12}$/C under air atmosphere with a heating rate of 10 °C min^{-1}.

Fig. 3 shows the laser Raman spectra of the as-synthesized $Li_4Ti_5O_{12}$/C composite. Two main bands were observed at around 1350 and 1580 cm^{-1}, which are designated as the D band and the G band, respectively. The G band is associated with the allowed E_{2g} optical modes of the Brillouin zone center of the crystalline graphite, while the D band is attributed to disorder-allowed phonon modes. The ratio can give information about the perfection of the graphite layer structure, As the I_D/I_G ratio increases, the defect structure increases and the degree of graphitization becomes less. The value of the I_D to I_G ratio of 1.99 was calculated. It suggests that the carbon was mainly in an amorphous structure.

The amount of coated carbon in $Li_4Ti_5O_{12}$/C composite was then determined by the TGA method. Shown in Fig. 4 is the TGA curve of the $Li_4Ti_5O_{12}$/C composite performed in a flowing air atmosphere. There was only a slight weight loss before 360 °C, a fast weight loss between 400 and 450 °C, and almost no further weight loss at temperature higher than 500 °C. Based on the TGA result, the carbon content in the $Li_4Ti_5O_{12}$/C was turned out around 3.35 wt.%.

As compared to the pristine $Li_4Ti_5O_{12}$, the $Li_4Ti_5O_{12}$/C composite was conducted additional calcination at 700 °C in nitrogen atmosphere for 2 h. Based on the results in Fig. 4, such additional calcination did not increase the grains size of $Li_4Ti_5O_{12}$ obviously. To further demonstrate its effect on the grain growth of $Li_4Ti_5O_{12}$, the surface area of pristine $Li_4Ti_5O_{12}$ prepared from the calcination of primary powder at 700 °C for 5 h ($Li_4Ti_5O_{12}$–5 h), or at 700 °C for 7 h ($Li_4Ti_5O_{12}$–7 h), or first calcination at 700 °C for 5 h, cooling to room temperature, and then recalcination at 700 °C for additional 2 h ($Li_4Ti_5O_{12}$–5 h–2 h), was measured by BET method with the results listed in Table 1. It is 3.1, 3.9 and 3.0 m^2 g^{-1} for $Li_4Ti_5O_{12}$–5 h, $Li_4Ti_5O_{12}$–7 h and $Li_4Ti_5O_{12}$–5 h–2 h, respectively. It suggests the calcination time did not cause a significant effect on the grain growth of $Li_4Ti_5O_{12}$. Sucrose would further suppresses the grain growth of $Li_4Ti_5O_{12}$ when it was introduced during the synthesis. So it is reasonable to assume that the grain size and the surface area of $Li_4Ti_5O_{12}$ phase in as-synthesized $Li_4Ti_5O_{12}$/C composite is the same to the pristine $Li_4Ti_5O_{12}$. The grain size was then calculated from the specific surface area by assuming the sphere shape of $Li_4Ti_5O_{12}$ with the results listed also in Table 1. A grain size of

Table 1
BET and grain size from BET of $Li_4Ti_5O_{12}$ and $Li_4Ti_5O_{12}$/C anodes prepared by cellulose-assisted combustion process calcined at 700 °C for 5 h and 7 h in air.

	BET (m^2 g^{-1})	Grain size (BET) (μm)
$Li_4Ti_5O_{12}$–5 h	3.1	0.9
$Li_4Ti_5O_{12}$–7 h	3.9	0.7
$Li_4Ti_5O_{12}$–5 h–2 h	3.0	0.9
$Li_4Ti_5O_{12}$/C–I	7.6	–

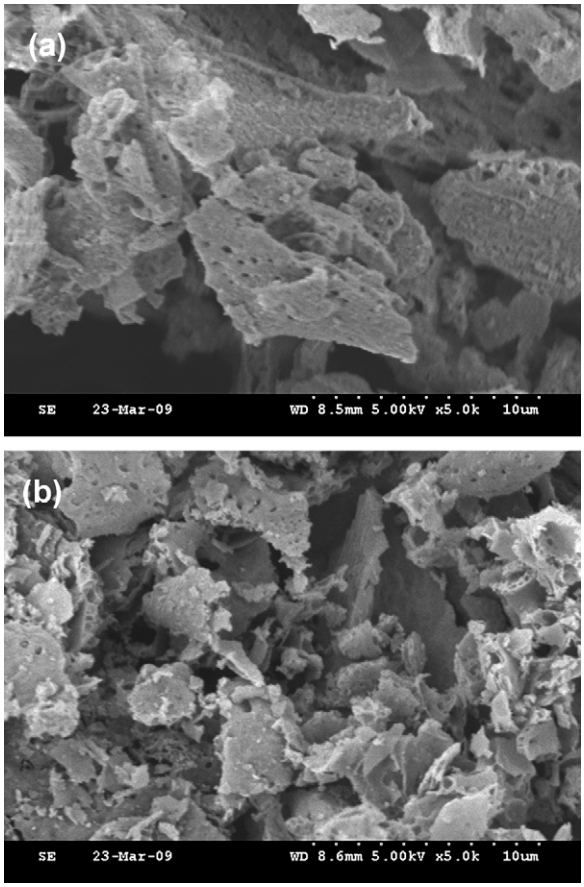

Fig. 5. SEM images of the (a) pristine $Li_4Ti_5O_{12}$ and (b) $Li_4Ti_5O_{12}$/C composite.

around 0.9 μm was calculated for the pristine $Li_4Ti_5O_{12}$. For the $Li_4Ti_5O_{12}$/C composite, a surface area of 7.6 m^2 g^{-1} was measured, which is about two times that of the pristine $Li_4Ti_5O_{12}$. The larger specific surface area of $Li_4Ti_5O_{12}$/C than $Li_4Ti_5O_{12}$ is due to the contribution from the coated carbon. Based on the amount of the carbon coating as determined by the TGA analysis and the specific surface area of the pristine $Li_4Ti_5O_{12}$, the specific surface area of the coated carbon was calculated to be around 114 m^2 g^{-1}. It suggests the coated carbon is in highly porous structure. Such porous carbon facilitated the diffusion of liquid electrolyte to the electrode surface, which is of critical importance for practical application. Based on the density of amorphous carbon of 1.90 ± 0.05 g cm^{-3} [32] and the grain size of $Li_4Ti_5O_{12}$ of 0.9 μm, the carbon layer thickness was found to be around 5 nm, which is much smaller than the grain size

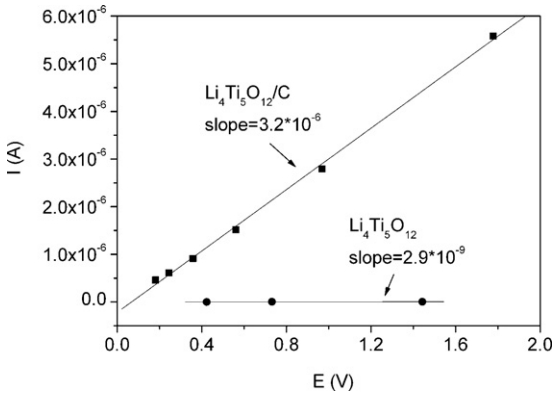

Fig. 6. Electrical conductivity of $Li_4Ti_5O_{12}$ and $Li_4Ti_5O_{12}$/C at room temperature.

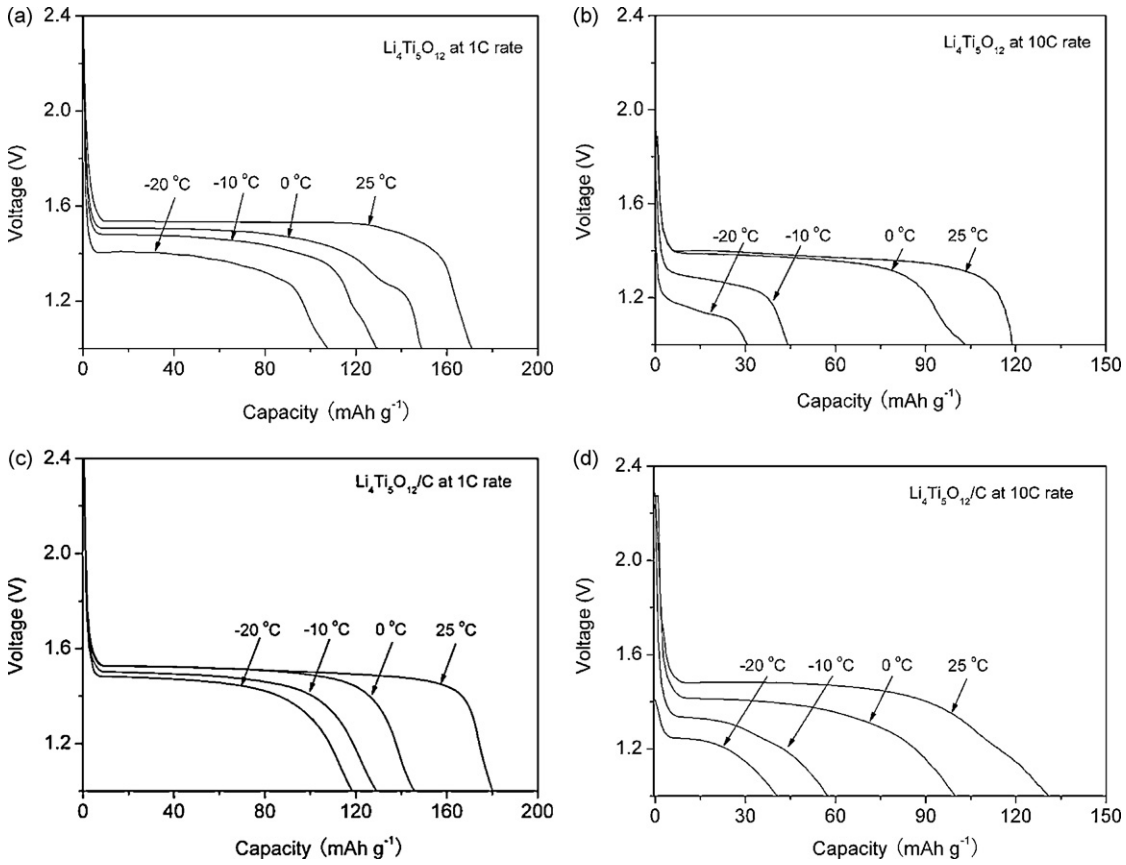

Fig. 7. The discharge profiles of the $Li_4Ti_5O_{12}$ anode (a) at 1 C rate; (b) at 10 C rate at various temperatures and $Li_4Ti_5O_{12}$/C anode (c) at 1 C rate; (d) at 10 C rate at various temperatures.

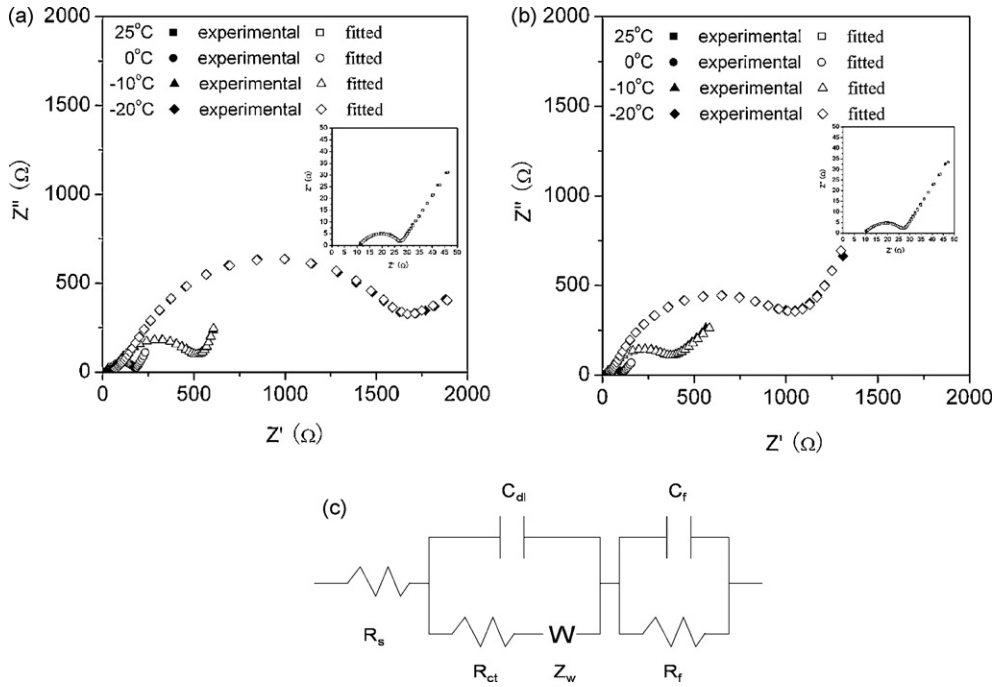

Fig. 8. EIS of (a) $Li_4Ti_5O_{12}$, (b) $Li_4Ti_5O_{12}$/C at various temperatures at the state of discharging (1.6 V), and (c) equivalent circuit. R_s: electrolyte resistance; R_{ct}: charge transfer resistance at the surface film-active material interface; R_f: surface polarization resistance; C_{dl}: double-layer capacitance of the electrode–electrolyte interface; C_f: surface capacitance; Z_w: Warburg impedance.

of $Li_4Ti_5O_{12}$. In the literature, a similar thickness of 2–10 nm was observed for $LiFePO_4$/C with about 2–5 wt.% carbon content [33].

Fig. 5 shows the SEM images of the pristine $Li_4Ti_5O_{12}$ and $Li_4Ti_5O_{12}$/C composite. Both samples had similar morphology of sponge shape with tremendous enclosed pores, which were attributed to huge amount of gaseous products formed during the auto-combustion process. Compared to the grain size calculated based on BET specific surface area, the grain size in SEM images is much larger. It suggests there was soft aggregation within the $Li_4Ti_5O_{12}$ powder. The successful deposition of carbon over the $Li_4Ti_5O_{12}$ was further supported by the substantial increment in the apparent conductivity of the oxide. The powder was formed into bar-shape pellets by die pressing, silver paste was adopted as the electrodes and silver wires as the current leads. 4-probe DC method was applied for the DC conductivity measurement. For the pristine $Li_4Ti_5O_{12}$, an electrical conductivity of 2.9×10^{-9} S cm^{-1} was obtained, which is similar to the literature result [8,34]. With the formation of $Li_4Ti_5O_{12}$/C composite, an electrical conductivity of 3.2×10^{-6} S cm^{-1} was obtained. As shown in Fig. 6, the electrical conductivity of $Li_4Ti_5O_{12}$/C is more than three orders higher than the pristine $Li_4Ti_5O_{12}$. The substantial increase in electrical conductivity is due to carbon distribution, i.e., covering on the surface of $Li_4Ti_5O_{12}$ grains.

3.2. Electrochemical performance

To test their electrochemical performance at low temperature, the pristine $Li_4Ti_5O_{12}$ and $Li_4Ti_5O_{12}$/C composite were assembled into half cells with metallic lithium film as the counter electrode and also reference electrode. The charge/discharge curves of the cells at 1 and 10 C rates at various temperatures between 25 and −20 °C are shown in Fig. 7. At 1 C rate, pristine $Li_4Ti_5O_{12}$ and $Li_4Ti_5O_{12}$/C composite show similar discharge/charge capacity at −10, 0, and 25 °C. However, $Li_4Ti_5O_{12}$/C (119 mAh g^{-1}) showed slightly higher discharge capacity than pristine $Li_4Ti_5O_{12}$ (108 mAh g^{-1}) at −20 °C. At 10 C rate, $Li_4Ti_5O_{12}$/C as a whole showed slightly higher discharge/charge capacity than the pristine $Li_4Ti_5O_{12}$ at all temperatures ranged from −20 to 25 °C. For example, it is 31 mAh g^{-1} for $Li_4Ti_5O_{12}$ at −20 °C as a comparison of 41 mAh g^{-1} for $Li_4Ti_5O_{12}$/C at the same temperature. It suggests the carbon coating is beneficial in improving the electrochemical performance at low temperature and high rate. For both pristine $Li_4Ti_5O_{12}$ and $Li_4Ti_5O_{12}$/C composite anodes, the electrode performance at low temperature and high rate is still highly attractive (108–119 mAh g^{-1} at 1 C rate and −20 °C), which is likely associated with the fine particle size from the reduced temperature synthesis.

To further demonstrate the effect of carbon coating on the electrode performance, the EIS of $Li_4Ti_5O_{12}$ and $Li_4Ti_5O_{12}$/C composite at the state of discharging (1.6 V) at various temperatures were measured. As shown in Fig. 8, all the EISs in Nyquist plot are comprised of a depressed semicircle in high to medium frequency range and a tail in the low frequency range. The high frequency intercept at the real axis corresponds to the ohmic resistance of the cell mainly contributed from the electrolyte and electrode, while the semicircle in the middle frequency range is mainly related to the complicated electrochemical reactions occurring at the electrolyte/cathode interface, which may include the charge-transfer resistance (both electron and lithium ion), particle-to-particle contact resistance, and corresponding capacitances. The inclined line in the lower frequency range is attributed to the Warburg impedance, which is associated with solid-state diffusion of Li ions through the bulk of $Li_4Ti_5O_{12}$. Fig. 8 clearly shows the cell electrochemical resistance comes mainly from the complicated electrochemical reactions over the $Li_4Ti_5O_{12}$ electrode surface. At 25 °C, comparable electrode polarization resistance of 27 and 26 Ω was observed for $Li_4Ti_5O_{12}$ and $Li_4Ti_5O_{12}$/C, respectively. With the decrease of operation temperature, this polarization resistance increased substantially, this is due to the reduced surface reaction kinetics. The pristine $Li_4Ti_5O_{12}$ showed a larger electrode polarization than $Li_4Ti_5O_{12}$/C composite, for example, they are 1700 and 1000 Ω at −20 °C, respectively, which suggests the carbon coating is effective in improving the electrode reaction kinetics at reduced operation temperature. Furthermore, the Nyquist plot with the equivalent circuit was shown in Fig. 8c. The impedance parameters of R_s, R_{ct} and R_f at different temperatures were listed in Table 2. As can be seen clearly in Table 2, with decreasing the temperature, the resistances of both $Li_4Ti_5O_{12}$ and $Li_4Ti_5O_{12}$/C electrodes increased gradually. However, the charge transfer resistances R_{ct} increased the fastest. It suggests the decrease of temperature has much more pronounced influence on the charge-transfer reaction occurring at the electrode/electrolyte interface. This conclusion agrees well with the observation of Liao et al. [35].

Table 2
Impedance parameters derived using equivalent circuit model and lithium diffusion coefficient D for $Li_4Ti_5O_{12}$ and $Li_4Ti_5O_{12}$/C electrode (at discharging state of 1.6 V).

	Temperature (°C)	R_s (Ω)	R_{ct} (Ω)	R_f (Ω)	D (cm^2 s^{-1})
$Li_4Ti_5O_{12}$	25	6.0	45.3	2.0	2.8×10^{-13}
	0	8.5	358.6	10.9	2.3×10^{-14}
	−10	16.3	1208.0	4.1	6.4×10^{-15}
	−20	56.4	2943.0	2.3	3.3×10^{-16}
$Li_4Ti_5O_{12}$/C	25	3.5	50.9	4.5	2.4×10^{-13}
	0	8.0	144.9	12.6	3.0×10^{-14}
	−10	14.3	347.9	20.5	1.7×10^{-15}
	−20	22.0	993.4	39.2	2.8×10^{-16}

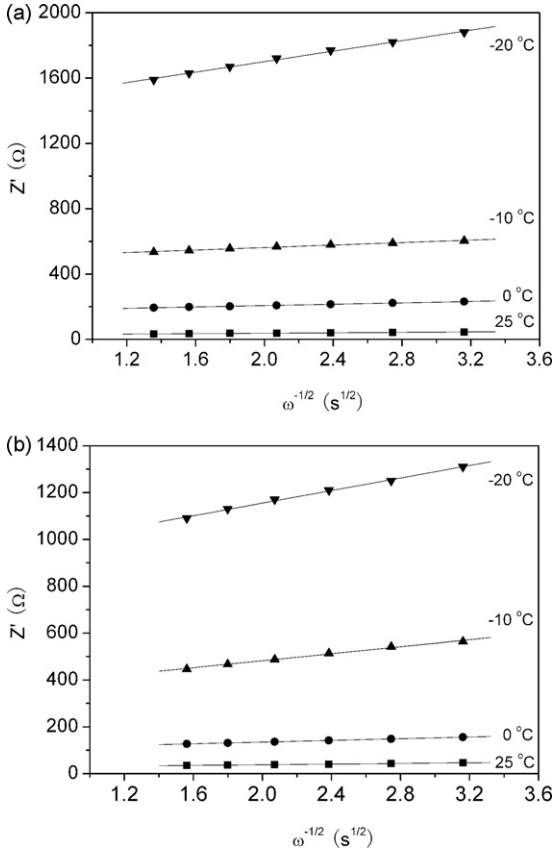

Fig. 9. Graph of Z' plotted against $\omega^{-1/2}$ at low frequency region for $Li_4Ti_5O_{12}$ and $Li_4Ti_5O_{12}$/C electrode (at the discharging stage of 1.6 V) at various temperatures.

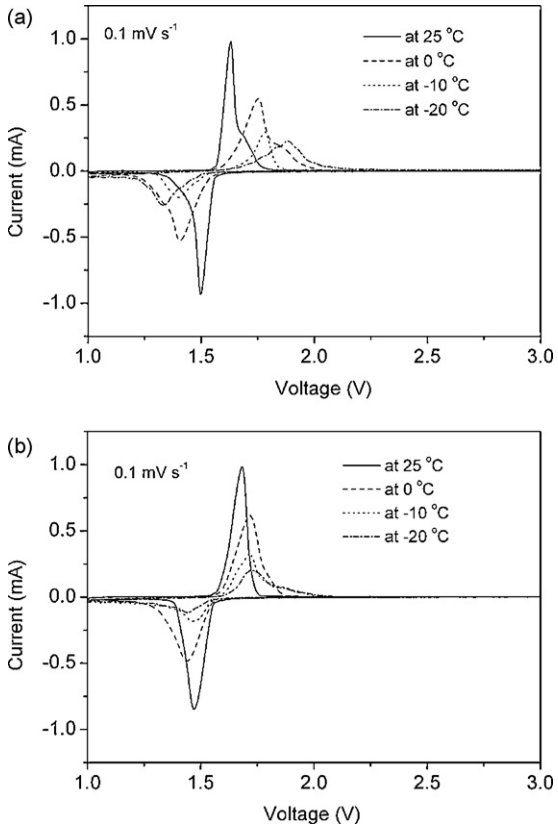

Fig. 10. Cyclic voltammograms of (a) $Li_4Ti_5O_{12}$ and (b) $Li_4Ti_5O_{12}$/C at various temperatures at a sweep rate of 0.1 mV s^{-1}.

The lithium-ion diffusion coefficient is calculated according to the following equation [35,36]:

$$D = \frac{R^2T^2}{2A^2n^4F^4C^2\sigma^2} \quad (1)$$

where the meanings of n is the number of electrons per molecule during oxidization, A the surface area of the electrode, D the diffusion coefficient of lithium ion, R the gas constant, T the absolute temperature, F the Faraday constant, C the concentration of lithium ion (C = 0.014 mol cm^{-3} for x = 1), and σ is the Warburg factor which has relationship with Z_{re}:

$$Z' = R_s + R_{ct} + R_f + \sigma\omega^{-1/2} \quad (2)$$

The graph of Z' against $\omega^{-1/2}$ in the low frequency region is a straight line with the slope of σ. The $Z' - \omega^{-1/2}$ plots at different temperatures were presented in Fig. 9. The lithium diffusion coefficients (D) for $Li_4Ti_5O_{12}$ and $Li_4Ti_5O_{12}$/C electrodes were calculated with the results also shown in Table 2. It clearly shows that a decrease in operation temperature resulted in a decrease in lithium diffusion coefficient. However, the value of lithium diffusion coefficient between $Li_4Ti_5O_{12}$ and $Li_4Ti_5O_{12}$/C electrodes was similar.

Recently, based on careful analysis of nine papers by different research groups, Gaberscek et al. claimed that in $LiFePO_4$-based cathode materials, a cathode material similar to $Li_4Ti_5O_{12}$ anode with a poor lithium-ion and electronic conductivity and a two-phase mechanism for lithium insertion and extraction, the electrode resistance depends solely on the mean particle size and the effect of carbon coating is marginal [37]. Kavan et al. have studied the particle size effect in spinel $Li_4Ti_5O_{12}$ [38], and they found that the Li-diffusion coefficients are strongly dependent on the particles size. As demonstrated previously, the grain size effects of $Li_4Ti_5O_{12}$ and $Li_4Ti_5O_{12}$/C are similar in current research. However,

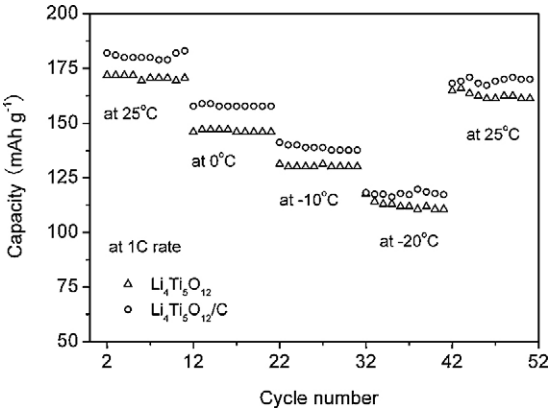

Fig. 11. Cycling performance of the $Li_4Ti_5O_{12}$ and $Li_4Ti_5O_{12}$/C at room and low temperatures.

it was observed that the $Li_4Ti_5O_{12}$/C electrode had better electrochemical performance than pristine $Li_4Ti_5O_{12}$ at low temperature, especially at high discharge rate. It implies the carbon coating does affect the electrochemical performance. Such improvement can be explained by the improved electrical wiring of the anode particles through the carbon coating of the $Li_4Ti_5O_{12}$.

Shown in Fig. 10 are the CV of pristine $Li_4Ti_5O_{12}$ and $Li_4Ti_5O_{12}$/C between 1.0 and 3.0 V with a voltage scan rate of 0.1 mV s^{-1} at different operation temperatures varied from 25 °C to −20 °C. At 25 °C, both pristine $Li_4Ti_5O_{12}$ and $Li_4Ti_5O_{12}$/C composite show a pair of sharp and reversible redox peaks, indicating the good electrode kinetic of both anodes. During the cathodic sweep, lithium ions are inserted in $Li_4Ti_5O_{12}$/C. A cathodic peak occurred at around 1.5 V versus Li^+/Li, corresponding to the flat voltage of discharge process. The voltage difference between anodic and cathodic peaks reflects the polarization degree of the electrode. With the decrease of operation temperature, the anodic peak and cathodic peak became broader, the peak current was reduced, and the voltage separation between the anodic peak and cathodic peak was enlarged. All above phenomena suggested worsened electrode kinetics with reduced operation temperature. As compared to the pristine $Li_4Ti_5O_{12}$, the anodic peak and cathodic peak of $Li_4Ti_5O_{12}$/C anode at reduced operation temperature are more symmetric and the voltage separation between anodic peak and cathodic peak is smaller, suggesting higher electrode activity of $Li_4Ti_5O_{12}$/C composite than pristine $Li_4Ti_5O_{12}$, agreeing well with the EIS results.

Fig. 11 shows the cycling stability of both pristine $Li_4Ti_5O_{12}$ and $Li_4Ti_5O_{12}$/C electrodes at various conditions at 1 C rate. Both electrodes show relatively stable cycling stability within the 50 cycles. The good cycling stability can be attributed to the near zero volume variation during the charge/discharge process.

4. Conclusions

With sucrose as organic carbon source, a thin layer of carbon has been successfully coated on the $Li_4Ti_5O_{12}$ anode material with the formation of phase-pure $Li_4Ti_5O_{12}$/C composite after the calcination at 700 °C in an inert atmosphere for 2 h, if the crystallized $Li_4Ti_5O_{12}$ phase was pre-formed. The surface carbon layer is amorphous, highly porous, around 5 nm in thickness, and around 3.35 wt.% in the $Li_4Ti_5O_{12}$/C composite. The conductivity of the $Li_4Ti_5O_{12}$ increased around 3 orders after the carbon coating. Both the pristine $Li_4Ti_5O_{12}$ material and $Li_4Ti_5O_{12}$/C composite showed good electrochemical performance at room temperature and low charge/discharge rates primarily because of the fine particle size thanks to the reduced temperature via the cellulose-assisted combustion process. Improved electrochemical charge/discharge

performance at reduced temperature and/or high charge/discharge rate were achieved by surface coating of the $Li_4Ti_5O_{12}$ with carbon. It is likely due to the increased electrical wiring efficiency of the anode particles. It suggests that the carbon coating is beneficial to improve the overall electrode activity and kinetics process, and the composites are more promising for low temperature and high rate applications.

Acknowledgements

This work was supported by the "Outstanding Young Scholar Grant at Jiangsu Province" under 306 contract No. 2008023 and the National Basic Research Program of China under contract No. 307 2007CB209704.

References

[1] E. Ferg, R.J. Gummov, A.de. Kock, M.M. Thackeray, J. Electrochem. Soc. 141 (1994) L147.
[2] K. Zaghib, M. Simoneau, M. Armand, M. Gauthier, J. Power Sources 81–82 (1999) 300.
[3] M. Kalbac, M. Zukalova, L. Kavan, J Solid State Eletrochem. 8 (2003) 2.
[4] T. Tabuchi, H. Yasuda, M. Yamachi, J. Power Sources 162 (2006) 813.
[5] T. Ohzuku, A. Ueda, N. Yamamoto, J. Electrochem. Soc. 142 (1995) 1431.
[6] D. Peramunage, K.M. Abraham, J. Electrochem. Soc. 145 (1998) 2609.
[7] K. Zaghib, M. Armand, M. Gauthier, J. Electrochem. Soc. 145 (1998) 3135.
[8] C.H. Chen, J.T. Vaughey, A.N. Jansen, D.W. Dees, A.J. Kahaian, T. Goacher, M.M. Thackeray, J. Electrochem. Soc. 148 (2001) A102.
[9] K. Nakahara, R. Nakajima, T. Matsushima, H. Majima, J. Power Sources 117 (2003) 131.
[10] Y.J. Hao, Q.Y. Lai, J.Z. Lu, X.Y. Ji, Ionics 13 (2007) 369.
[11] A. Singhal, G. Skandan, G. Amatucci, F. Badway, N. Ye, A. Manthiram, H. Ye, J.J. Xu, J. Power Sources 129 (2004) 38.
[12] Z.Y. Wen, X.L. Yang, S.H. Huang, J. Power Sources 174 (2007) 1041.
[13] L. Kavan, M. Grätzel, Electrochem. Solid-State Lett. 5 (2002) A39.
[14] D.H. Kim, Y.S. Ahn, J. Kim, Electrochem. Commun. 7 (2005) 1340.
[15] S.S. Lee, K.T. Byun, J.P. Park, S.K. Kim, H.Y. Kwak, I.W. Shim, Dalton Trans. 37 (2007) 4182.
[16] Y. Abe, E. Matsui, M. Senna, J. Phys. Chem. Solids 68 (2007) 681.
[17] J. Kim, J. Cho, Electrochem. Solid State Lett. 10 (2007) A81.
[18] J.R. Li, Z.L. Tang, Z.T. Zhang, Electrochem. Commun. 7 (2005) 894.
[19] T. Yuan, R. Cai, K. Wang, R. Ran, S.M. Liu, Z.P. Shao, Ceram. Int. 35 (2009) 1757.
[20] S.H. Huang, Z.Y. Wen, J.C. Zhang, X.L. Yang, Electrochim. Acta 52 (2007) 3704.
[21] S.H. Huang, Z.Y. Wen, X.J. Zhu, X.L. Yang, J. Electrochem. Soc. 152 (2005) A1301.
[22] G.J. Wang, J. Gao, L.J. Fu, N.H. Zho, Y.P. Wu, T. Takamura, J. Power Sources 174 (2007) 1109.
[23] H. Liu, Y. Feng, K. Wang, J.Y. Xie, J. Phys. Chem. Solids 69 (2008) 2037.
[24] J. Gao, J.R. Ying, C.Y. Jiang, C.R. Wan, J. Power Sources 166 (2007) 255.
[25] L. Cheng, X.L. Li, H.J. Liu, H.M. Xiong, P.W. Zhang, Y.Y. Xia, J. Electrochem. Soc. 154 (2007) A692.
[26] J.L. Allen, T.R. Jow, J. Wolfenstine, J. Power Sources 159 (2006) 1340.
[27] T. Yuan, K. Wang, R. Cai, R. Ran, Z.P. Shao, J. Alloys Compd. 477 (2009) 665.
[28] X.L. Yao, S. Xie, C.H. Chen, Q.S. Wang, J.H. Sun, Y.L. Li, S.X. Lu, Electrochim. Acta 50 (2005) 4076.
[29] K. Wang, R. Cai, T. Yuan, X. Yu, R. Ran, Z.P. Shao, Electrochim. Acta 54 (2009) 2861.
[30] T. Yuan, R. Cai, R. Ran, Y.K. Zhou, Z.P. Shao, J. Mater. Res., submitted for publication.
[31] E. Pretsch, P. Bühlmann, C. Affolter, Structure Determination of Organic Compounds Tables of Spectral Data, Springer-Verlag: Berlin, 2000, p. 13 (Chapter 1).
[32] C. Martin, E.T. Arakawa, T.A. Callcott, J.C. Ashley, J. Electron. Spectrosc. Relat. Phenom. 35 (1985) 307.
[33] R. Dominko, M. Gaberscek, M. Bele, D. Mihailovic, J. Jamnik, J. Eur. Ceram. Soc. 27 (2007) 909.
[34] H.Y. Yu, X.F. Zhang, A.F. Jalbout, X.D. Yan, X.M. Pan, H.M. Xie, R.S. Wang, Electrochim. Acta 53 (2008) 4200.
[35] X.Z. Liao, Z.F. Ma, Q. Gong, Y.S. He, L. Pei, L.J. Zeng, Electrochem. Commun. 10 (2008) 691.
[36] A.J. Bard, L.R. Faulkner, Electrochemical Methods, Wiley, New York, 1980.
[37] M. Gaberscek, R. Dominko, J. Jamnik, Electrochem. Commun. 9 (2007) 2778.
[38] L. Kavan, J. Prochaïzka, T.M. Spitler, M. Kalbaïc˘, M. Zukalovaï, T. Drezen, M. Gra¨tzel, J. Electrochem. Soc. 150 (7) (2003) A1000.